Quaternary Science Reviews 343 (2024) 108916

Contents lists available at ScienceDirect

Quaternary Science Reviews

journal homepage: www.elsevier.com/locate/quascirev

Sea ice in the Nordic Seas: Greenland stadial to interstadial changes

Wanyee Wong [a,*], Bjørg Risebrobakken [a], Kirsten Fahl [c], Ruediger Stein [c,d,e], Eystein Jansen [a,b], Kristine Steinsland [a], Catherine Kissel [f]

[a] NORCE Norwegian Research Centre, Bjerknes Centre for Climate Research, 5007, Bergen, Norway
[b] Department of Earth Science, University of Bergen, Bjerknes Centre for Climate Research, 5007, Bergen, Norway
[c] Alfred Wegener Institute, Helmholtz Centre for Polar and Marine Research, 27568, Bremerhaven, Germany
[d] Faculty of Geosciences (FB5) and Center for Marine Environmental Sciences (MARUM), University of Bremen, 28359, Bremen, Germany
[e] Key Laboratory of Marine Chemistry Theory and Technology, Ocean University of China, 266100, Qingdao, China
[f] Laboratoire des Sciences du Climat et de l'Environnement, CEA-CNRS-UVSQ, Université Paris-Saclay, 91190, Gif-sur-Yvette, France

ARTICLE INFO

Handling editor: C. O'Cofaigh

Keywords:
Sea ice extent
Dansgaard-Oeschger events
Abrupt climate change
Lipid biomarkers
Fram Strait

ABSTRACT

Sea ice conditions in the eastern Fram Strait between 40 and 36.5 ka b2k (thousand years before the year 2000) are reconstructed in detail, based on biomarker analyses. Following extensive sea ice conditions around the Greenland Interstadial 9/Greenland Stadial 9 transition at 39.9 ka b2k, repeated polynya activity marked Greenland Stadial 9 in the eastern Fram Strait. Nearly perennial sea ice was observed around the Greenland Stadial 9/Greenland Interstadial 8 transition at 38.22 ka b2k, followed by a gradual establishment of seasonal sea ice cover over the research area during Greenland Interstadial 8. Previous studies highlighted sea ice retreat in the southeastern Nordic Seas as a driver of abrupt Greenland Stadial to Interstadial climate change. We document intervals with less sea ice in the eastern Fram Strait during Greenland Stadial 9 and Interstadial 8 than previously suggested. By mapping the variable sea ice extent during Greenland Stadial 9 and Interstadial 8, further constraints are detected that may help define the role of the Nordic Seas sea ice cover in driving abrupt climate change during glacial times.

1. Introduction

The Dansgaard-Oeschger (D-O) events of the Last Glacial Period are characterized by abrupt warming from cold Greenland Stadials (GSs) to relatively mild Greenland Interstadials (GIs) in the Greenland ice cores and marine sediment cores from the North Atlantic region and adjacent continents. Following the warmest early stage of GIs, gradual cooling occurred, with abrupt cooling to full GS conditions by the end of GIs (Rasmussen et al., 2014).

Evidence suggests that the D-O events are closely linked to changes in the Nordic Seas sea ice cover (e.g., Dokken and Jansen, 1999; Zumaque et al., 2012; Dokken et al., 2013; Li and Born, 2019; Sadatzki et al., 2020). Sea ice dynamics influence the Earth's energy budget by changing the surface albedo, ocean-atmosphere heat and moisture exchange, and the ocean circulation that redistributes heat (Parmentier et al., 2013; Gao et al., 2015). With an extensive sea ice cover in the Nordic Seas, a strong halocline is formed, and warmer Atlantic Water (AW) is forced to submerge into intermediate water depths. The submerged AW contributes to the buildup of an ocean heat reservoir beneath the halocline (e.g., Rasmussen and Thomsen, 2004; Ezat et al., 2014; Sadatzki et al., 2019; El bani Altuna et al., 2021), since the sea ice cover restricts the ocean heat loss to the atmosphere (Hoff et al., 2016). When the Nordic Seas is free of sea ice, heat and moisture exchange between the ocean and the atmosphere takes place further north towards the Arctic, leading to a warmer climate in the high latitudes relative to the periods when sea ice covers the Nordic Seas (Hoff et al., 2016). Furthermore, changes in the Nordic Seas sea ice distribution affect the North Atlantic Deep Water (NADW) formation, which is an important component of the Atlantic Meridional Overturning Circulation (AMOC) (Dokken et al., 2013; Menviel et al., 2020). Sea ice therefore plays a vital role in regional and global climate oscillations through its impact on ocean-ice-atmosphere interactions.

In the southeastern Nordic Seas, paleoclimatic proxy data show that seasonal sea ice prevailed during GSs (Hoff et al., 2016; Sadatzki et al., 2020). It is also suggested that the AMOC weakened during the GSs (McManus et al., 1999; Henry et al., 2016; Sadatzki et al., 2020). Sea ice retreat in the southeastern Nordic Seas preceded the Greenland warming and the major reinvigoration of the AMOC during the GS-GI transitions

* Corresponding author.
E-mail address: yunw@norceresearch.no (W. Wong).

https://doi.org/10.1016/j.quascirev.2024.108916
Received 5 June 2024; Received in revised form 9 August 2024; Accepted 17 August 2024
Available online 2 September 2024

(Sadatzki et al., 2019). After a rapid (<250 years) large-scale reduction of sea ice in the southeastern Nordic Seas (Berben et al., 2020; Sadatzki et al., 2020), relatively warm AW reached the sea surface, preventing sea ice from expanding southwards during GIs (Sadatzki et al., 2019; Sessford et al., 2019). In the northern Nordic Seas, extensive sea ice is suggested to prevail during most of the D-O cycles, based on relatively low-resolution biomarker data (El bani Altuna et al., 2024).

Yet, there is a lack of knowledge regarding the extent and duration of sea ice coverage in the Nordic Seas during the GSs, GIs, and GS-GI transitions. To understand the mechanics of ocean-ice-atmosphere interactions during D-O climate oscillations, it is necessary to examine direct evidence of sea ice changes in the northern Nordic Seas with higher temporal resolutions to supplement evidence from further south. Here, we address this knowledge through high-resolution reconstructions of sea ice conditions in the eastern Fram Strait during GS-9 and GI-8. Our reconstructions rely on lipid biomarker proxies, specifically, paired records of highly branched isoprenoids (HBIs) (i.e., IP_{25} and HBI-III (Z)) and sterols (i.e., brassicasterol, dinosterol, campesterol and sitosterol) from marine sediment core MD99-2304 in the eastern Fram Strait (1348 m water depth; 77°37′15.6″N 9°56′54″E) (Fig. 1).

IP_{25} is biosynthesized by spring sea ice diatoms (Belt et al., 2007; Brown et al., 2014). HBI-III (Z) is derived from pelagic phytoplankton but has enhanced abundance near the marginal ice zones (MIZ) in the Arctic realm (Belt et al., 2015; Smik et al., 2016). Here, MIZ is defined as the oceanographic front between the main sea ice cover and ice-free areas (Dumont, 2022). Brassicasterol and dinosterol are known for their occurrence in pelagic, open ocean conditions (Volkman, 2006; Stoynova et al., 2013; Kolling et al., 2020; Su et al., 2022). Campesterol and sitosterol are commonly ascribed to terrestrial vascular plants (Fahl and Stein, 2007; Müller et al., 2009; Bianchi and Canuel, 2011), and are combined as an identifier of terrestrial organic matter. A thick sea ice cover inhibits sunlight from penetrating through, leading to low IP_{25} concentrations, comparable to the values seen under ice-free conditions (e.g., Müller et al., 2011; Smik et al., 2016; Stein et al., 2017). To differentiate between perennial sea ice cover and open water conditions, we apply the PIP_{25} indices (open water phytoplankton biomarker-IP_{25}, see Formula I and II in Material and methods) (Müller et al., 2011; Stein et al., 2017), which combine the data semi-quantitatively. Based on the mentioned lipid biomarker proxies and indices, we map the sea ice extent in the Nordic Seas from 40 to 36.5 ka b2k with unprecedented details. Gaining a comprehensive understanding of how abrupt changes in sea ice affect regional and global climate is key to helping improve future projections.

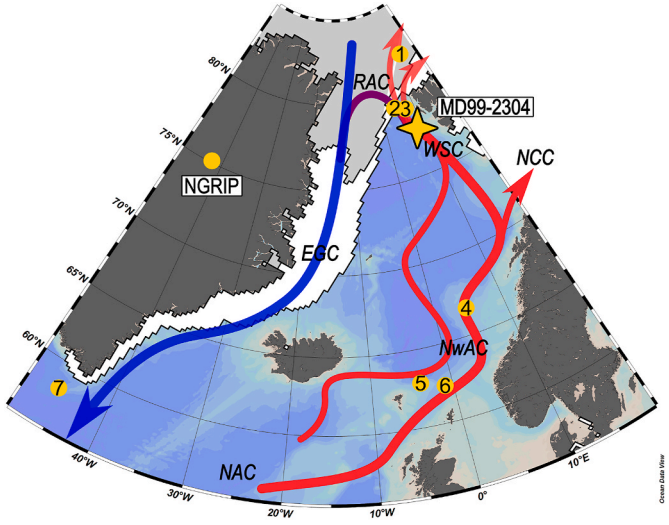

Fig. 1. Map showing the research area and core sites with available biomarker data covering the investigated time interval (40–36.5 ka b2k). The yellow star represents Core MD99-2304. The yellow dots represent sites used for comparison: (1) PS92/039-2 (Kremer et al., 2018b), (2) PS93/006-1 (Kremer et al., 2018a), (3) HH15-1252 PC (El bani Altuna et al., 2021; 2024), (4) MD95-2010 (Sadatzki et al., 2020), (5) JM11-FI-19PC (Hoff et al., 2016), (6) MD99-2284 (Sadatzki et al., 2019), and (7) GS16-204-23-CC (Scoto et al., 2022). The coring sites were numbered according to their latitudes, from north to south. Grey areas mark the 2023 September sea ice extent, and white areas mark the 2023 March sea ice extent (Florence et al., 2017, updated by 2024). The red arrows illustrate the warm and saline North Atlantic Current (NAC), Norwegian Atlantic Currents (NwAC), West Spitsbergen Current (WSC), and North Cape Current (NCC). The blue arrow illustrates the cold and fresh East Greenland Current (EGC). The purple-blue branch illustrates the submerging Return Atlantic Current (RAC). The map was produced with Ocean Data View (https://odv.awi.de/) and Inkscape software (http://www.inkscape.org/).

2. Study area

2.1. Present day oceanography

The North Atlantic Current (NAC) enters the Norwegian Sea over the Greenland-Scotland Ridge and splits into the two-branched Norwegian Atlantic Current (NwAC). The NwAC flows northwards in the eastern Nordic Seas, bringing warm AW northwards along the continental slope of Norway (Bosse et al., 2018; Smedsrud et al., 2022). The eastern branch of the NwAC bifurcates in the northern Norwegian Sea. The North Cape Current (NCC) flows into the Barents Sea, and the West Spitsbergen Current (WSC) enters the eastern Fram Strait and is joined by the western branch of the NwAC (Fig. 1) (Bosse et al., 2018).

The Fram Strait is the major gateway for the exchange of water masses between the Arctic Ocean and the North Atlantic (Muilwijk et al., 2018). As AW moves poleward, it cools and densifies as heat is lost to the atmosphere. Due to this densification, the WSC submerges in the Fram Strait. While one part of the submerged WSC enters the Arctic Ocean, another part recirculates southward in the intermediate layer through the Return Atlantic Current (RAC) (Hattermann et al., 2016). In the western Fram Strait, the East Greenland Current (EGC) transports cold, fresh Polar Water (PW) southward from the Arctic Ocean along the east Greenland slope (Fig. 1) (Smedsrud et al., 2022). In between AW in the eastern, and PW in the western Nordic Seas, there is a mixture of these two water masses named Arctic Water (ArW) (Olafsson et al., 2021).

2.2. Present-day and future sea ice conditions

Over the last decades, the Arctic Ocean sea ice extent and thickness have seen a clear declining trend, including the amount of multi-year sea ice (Florence et al., 2017, updated by 2024; Notz and Stroeve, 2018; Parkinson and DiGirolamo, 2021). This retreat is accompanied by an abrupt atmospheric warming over the area of strong sea ice retreat and adjacent land areas (Jansen et al., 2020). The eastern Fram Strait is mostly ice-free, with open water reaching northwest of Svalbard during summers (Fig. 1) (Onarheim et al., 2018). Future projections show a further decline in the Arctic sea ice extent over the next century, as a response to anthropogenic emissions (e.g., Dörr et al., 2024; Jahn et al., 2024). At present, sea ice and freshwater are exported from the Arctic Ocean through the western Fram Strait and southwards in the western Nordic Seas, following EGC (Fig. 1) (Smedsrud et al., 2017).

The Northeast Water (NEW) Polynya, an area of open water surrounded by sea ice, is situated in the modern northwest Fram Strait (Barber and Massom, 2007; Bennett et al., 2024). Both latent (i.e., ice motions driven by physical forcing) and sensible heat processes (i.e., surface ocean heat fluxes) play significant roles in the formation of the NEW Polynya (Schneider and Budéus, 1997; Barber and Massom, 2007). The potential disappearance of the NEW polynya due to ongoing sea ice loss is discussed (Bennett et al., 2024; Jahn et al., 2024).

3. Material and methods

3.1. Chronological framework

The chronology of MD99-2304 is set by tuning the low field magnetic susceptibility (K_{lf}) of MD99-2304 to the K_{lf} of Core MD95-2010 from the Norwegian Sea (Kissel et al., 1999), adapting the MD95-2010 chronological framework from Sadatzki et al. (2020) (Figs. 1 & 2). The chronology of MD95-2010 (Sadatzki et al., 2020) is tied to the chronology of MD99-2284, a core located in the Faeroe-Shetland Channel (Fig. 1) (Berben et al., 2020). The MD99-2284 age model was originally constrained by tunning the anhysteretic remanent magnetization to the Greenland $\delta^{18}O$ (Dokken et al., 2013; Sadatzki et al., 2019), following the findings of Kissel et al. (1999) where they showed how oscillations in magnetic properties in the North Atlantic change in phase with the $\delta^{18}O$ of Greenland ice cores. The Greenland chronological framework used is the Greenland Ice Core Chronology 2005 (GICC05) (Andersen et al., 2006; Rasmussen et al., 2014; Seierstad et al., 2014). Later, the MD99-2284 chronology was further constrained by targeted high-resolution identification of cryptotephra (Berben et al., 2020). Six individual marine tephra horizons were identified between 32 and 40 ka b2k, from where four of these could be used as isochronous time markers between tephra horizons found in Greenland ice cores and MD99-2284.

The K_{lf} of all three cores was measured at the paleomagnetic laboratory at the LSCE in Gif-sur-Yvette. Measurements were done every 2 cm on u-channels, using a Bartington sensing coil with 5.5 cm diameter displaced along the u-channel sections. The K_{lf} is presented as K_{lf} (10^{-6} SI). The K_{lf} record from Core MD99-2010 was published in Kissel et al. (1999), while the K_{lf} records from MD99-2304 and MD99-2284 were not previously published.

The corresponding depths between MD99-2304 and MD95-2010 were identified, before adopting the MD95-2010 age-depth model from Sadatzki et al. (2020). Tie points are set for each transition, in and out of the GIs and GSs between 31.9 and 41.1 ka b2k (Fig. 2; Table 1). All ages are given as ka b2k.

In MD99-2304, an interval (916.25–905.25 cm, ca. 37.7 ka b2k) where 0.1 ± 0.2% of the sediment was >63 μm is interpreted to represent the fine-grained tail of a turbidite. When setting the chronology for MD99-2304, this interval is considered to have been deposited instantaneously. The signals recorded by this layer are therefore not representative of sea ice or climate history at the site and have been omitted from the records presented in this paper.

In the discussion, we compare our results to the records from HH15-1252 PC (3 in Fig. 1, El bani Altuna et al., 2021, 2024) and GS16-204-23CC (7 in Fig. 1, Scoto et al., 2022). The originally published chronologies of these cores are used, and all ages are given as ka b2k. For HH15-1252 PC, the GIs and GSs are recognized by correlating the planktic foraminiferal $\delta^{18}O$ to the NGRIP $\delta^{18}O$ at the GICC05 (El bani Altuna et al., 2021, 2024). Based on magnetic susceptibility and paleointensity, Scoto et al. (2022) adopted the chronological framework from PS2644, a core from the Denmark Strait where the age model is supported by numerous ^{14}C ages and identified tephra layers (Voelker et al., 2000; Voelker and Haflidason, 2015) and transferred to the GICC05. Hence, all records presented are set at the GICC05.

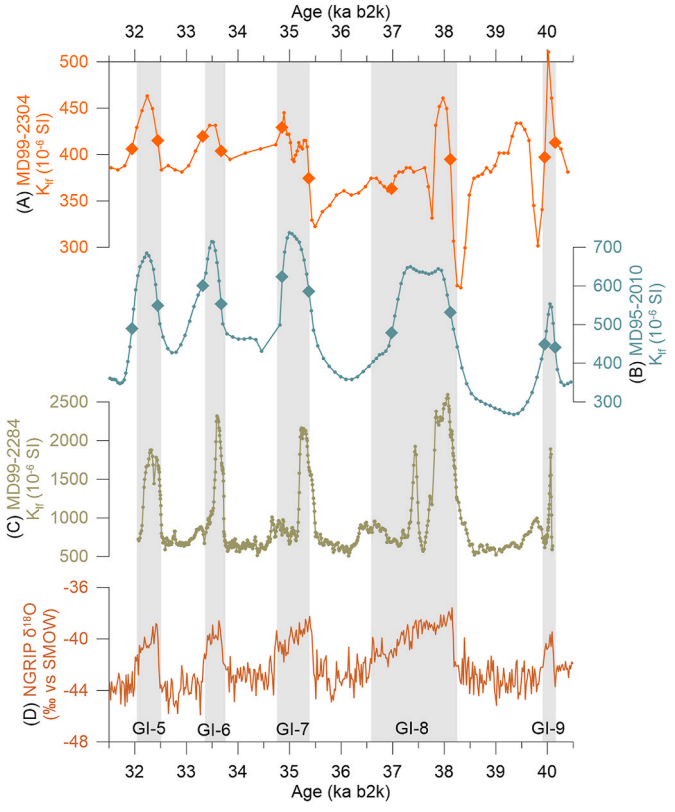

Fig. 2. Low field magnetic susceptibility (K_{lf}) of (A) MD99-2304, (B) MD95-2010 (Kissel et al., 1999), and (C) MD99-2284 shown on the same chronological framework. (D) NGRIP ice core (GICC05) 20 years mean $\delta^{18}O$ (North Greenland Ice Core Project members, 2004; Andersen et al., 2006), shown as a reference. The small dots in (A), (B) and (C) illustrate the data points, and the oval symbols in (A) and (B) represent the tie points used for tuning. For further details on the MD99-2284 and MD95-2010 age models, we refer to Berben et al. (2020) and Sadatzki et al. (2020).

3.2. Biomarker analysis

For MD99-2304, the depth interval between 937.75 and 895.75 cm (39.3–37.8 ka b2k) was analyzed every 0.5 cm (ca. 20 years/sample). The intervals of 974.25–937.75 cm (40–39.3 ka b2k) and 895.75–874.25 cm (37.8–36.5 ka b2k) were analyzed every 0.5–1 cm (ca. 20–40 years/sample). In total 149 samples were measured in this study. For normalizing biomarker concentrations, total organic carbon (TOC) was measured (90 mg of freeze-dried and homogenized sediment) in all samples using a Carbon-Sulfur Analyzer (CS-125, Leco) after removing carbonate with hydrochloric acid. All analyses were performed at the Alfred Wegener Institute (AWI) Bremerhaven, Germany.

The biomarkers were extracted from freeze-dried and homogenized sediment samples by ultrasonication for 15 min followed by centrifugation (2000 rpm, 4 min). This procedure was repeated three times using dichloromethane:methanol (2:1, v/v) as solvent. Prior to extraction, the internal standards 7-hexylnonadecane (7-HND, 0.066 μg, for IP_{25} quantification), 9-octylheptadec-8-ene (9-OHD, 0.1 μg, for different

Table 1
Tie points that are used to establish the chronological framework. The magnetic susceptibility of MD99-2304 was tuned to the magnetic susceptibility of MD95-2010, depth to depth, before adapting the MD95-2010 age model from Sadatzki et al. (2020). The corrected MD99-2304 depth refers to the depths in MD99-2304 after adjusting for the fine-grained turbidite tail sediment deposition. Linear interpolation sets the ages between the defined tie points.

MD99-2304 Original depth (cm)	MD99-2304 Corrected depth (cm)	Corresponding MD95-2010 Depth (cm)	Corresponding age (ka b2k) (Sadatzki et al., 2020)
783	783	708	31.943
793	793	720	32.443
807	807	731	33.315
813	813	740	33.672
823	823	753	34.858
855	855	764	35.375
885	885	783	36.983
927	915.5	802	38.119
973	961.5	823	39.948
979	967.5	829	40.146

quality control procedures), 5α-androstan-3β-ol (androstanol, 10.6 μg, for sterol), and 2,6,10,15,19,23-hexamethyltetracosane (squalane, 3.2 μg, for *n*-alkanes if needed later) were added to each sample. The total lipid extracts were separated by open silica (SiO_2) column chromatography with *n*-hexane (5 ml) and ethyl acetate:*n*-hexane (9 ml, 2:8 v/v) as eluent into the hydrocarbon and sterol fractions. The sterol fraction was silylated using 200 μl bis-trimethylsilyl-trifluoroacet-amide (BSTFA; 60 °C, 2 h).

The biomarkers were measured by gas chromatography/mass spectrometry (GC/MS) using an Agilent 7890B GC (30m DB-1MS column, 0.25 mm i.d., 0.25 μm film thickness) coupled to an Agilent 5977A mass selective detector (MSD, 70 eV constant ionization potential, Scan 50–550 m/z, 1 scan/s, ion source temperature 230 °C, Performance Turbo Pump), with selected ion monitoring mode (SIM) for HBIs and full scan mode (50–550 m/Z) for sterols. Here we present the data of sea ice proxy IP_{25} (C HBI monoene), HBI-III (Z) ($C_{25:3}$ Z-isomer), brassicasterol (24-methylcholesta-5,22E-dien-3β-ol), dinosterol (4a-23,24-trimethyl-5a-cholest-22E-en-3β-ol), campesterol (24-methylcholest-5-en-3β-ol), and sitosterol (24-methylcholest-5-en-3β-ol). These selected HBIs and sterols were identified based on the GC retention times compared to those of reference compounds as well as published mass spectra for HBIs (Belt et al., 2000, 2007) and for sterols (Boon et al., 1979; Volkman, 1986). HBIs were quantified based on their molecular ions (m/z 350 for IP_{25} and m/z 346 HBI-III (Z)) in relation to the fragment ion m/z 266 of 7-HND. Brassicasterol, dinosterol, campesterol, and sitosterol were quantified as trimethylsilyl ethers. The molecular ions m/z 470, 500, 472, and 486, respectively, were used in relation to the molecular ion m/z 348 of the internal standard androstanol. To balance different responses of molecular ions of the analytes and the molecular/fragment ions of the internal standards, an external calibration was applied (for further see Fahl and Stein (2012).

The semi-quantitative measure PIP_{25} is applied to differentiate between perennial sea ice and ice-free areas (Müller et al., 2011; Stein et al., 2017).

$$\text{I } PIP_{25} = \frac{IP_{25}}{(IP_{25} + (\text{phytoplankton biomarker} * c))}.$$

$$\text{II } c = \frac{\text{mean } IP_{25} \text{ concentration}}{\text{mean phytoplankton biomarker concentration}}.$$

The balance factor *c* is defined as the ratio between mean concentrations of IP_{25} and phytoplankton biomarkers (Müller et al., 2011). We present PIP_{25} values calculated with the phytoplankton biomarkers HBI-III (Z) ($P_{III}IP_{25}$), brassicasterol (P_BIP_{25}) and dinosterol (P_DIP_{25}). In this study, the PIP_{25} indices calibrated with a *c* based on the surface sediment samples from the Arctic Ocean and adjacent seas from Xiao et al. (2015) and Kolling et al. (2020) are not significantly different from the PIP_{25} calibrated with a regional *c* based on the downcore sediment samples of MD99-2304. Therefore, we adopt a regional factor *c*, with 2.82 for $P_{III}IP_{25}$, 0.025 for P_BIP_{25}, and 0.044 for P_DIP_{25} in this research.

PIP_{25} values are associated with modern spring/summer sea ice concentration according to the intercomparison between marine sediment biomarker records and satellite sea ice data. PIP_{25} values < 0.5 and >0.75 represent less ice and nearly perennial sea ice conditions respectively; while PIP_{25} values between 0.5 and 0.75 stand for seasonal ice cover/stable ice edge (Müller et al., 2011; Xiao et al., 2015; Stein et al., 2017).

To increase the temporal resolution of biomarker records from sediment core MD95-2010 around the GS-9/GI-8 transition (Sadatzki et al., 2020), TOC and biomarkers were analyzed in four additional samples (808–807, 804.5–803.5, 801.5–800.5, and 799.5–798.5 cm). Balance factor *c* remained 0.68 for $P_{III}IP_{25}$ and 0.013 for P_BIP_{25} in MD95-2010.

4. Results

In Core MD99-2304, biomarkers were detected in all analyzed samples. Between 40 and 39.6 ka b2k, biomarker concentrations were generally low (Figs. 3 & 4). Minima were recorded for HBI (i.e., IP_{25} and HBI-III (Z)) and sterol (i.e., brassicasterol, dinosterol, and campesterol+β-sitosterol) concentrations at 39.8 ka b2k. Following these minima, IP_{25} concentrations increased while HBI-III (Z) remained stably low (Fig. 3C). Brassicasterol and dinosterol concentrations increased after the minima (Fig. 3D). Between 40 and 39.6 ka b2k, mean$P_{III}IP_{25}$ value was 0.6, while mean P_BIP_{25} and P_DIP_{25} values were both 0.5 (Fig. 3E). Average concentration of campesterol+β-sitosterol during this time period was 18.8 μg/TOC% (Fig. 3F).

Between 39.6 and 38.5 ka b2k, HBI concentrations remained stable until 38.9 ka b2k. From 38.9 to 38.5ka b2k higher HBI concentrations and larger variability are recorded (Figs. 3C & 4). Meanwhile, sterols showed increased yet variable concentrations between 39.6 and 38.5 ka b2k (Figs. 3D & 4). During this time period, mean $P_{III}IP_{25}$ and P_DIP_{25} values were 0.5 while mean P_BIP_{25} was 0.4 (Fig. 3E) and the average concentration of campesterol+β-sitosterol was 33 μg/TOC% (Fig. 3F).

From 38.5 ka b2k, biomarker concentrations started to decrease (Figs. 3 & 4). At 38.4 ka b2k, minimum concentrations are documented for both HBIs and sterols, followed by an increase in the concentrations of all biomarkers (Fig. 3). Between 38.5 and 38.1 ka b2k, average values were 0.7 for both $P_{III}IP_{25}$ and P_BIP_{25}, and 0.6 for P_DIP_{25} (Fig. 3E). Campesterol+β-sitosterol had a mean concentration of 18.4 μg/TOC%

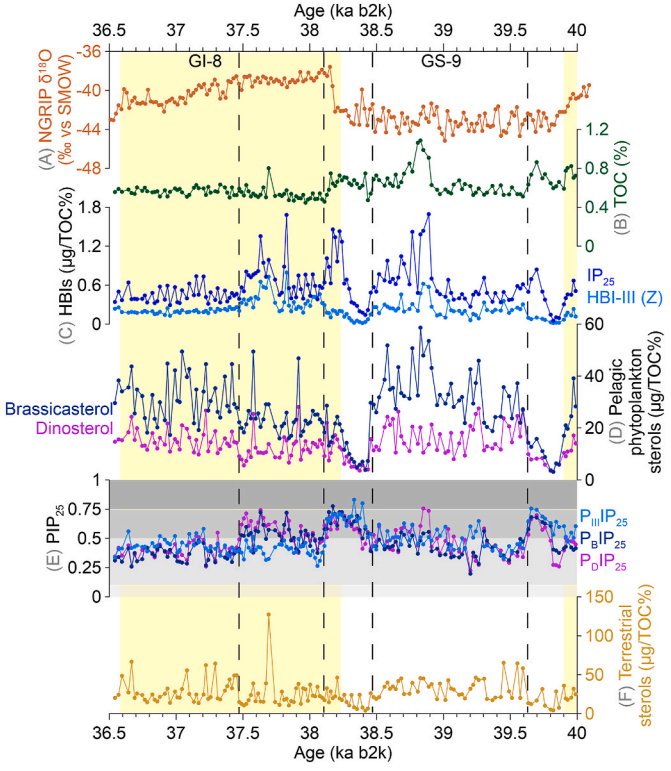

Fig. 3. Biomarker results from MD99-2304 with NGRIP oxygen isotopes as a reference. (A) NGRIP $\delta^{18}O$ (‰ vs SMOW) (20 years mean, GIC05 age model) (North Greenland Ice Core Project members, 2004; Andersen et al., 2006), (B) TOC, (C) HBIs (IP_{25} and HBI-III (Z)), (D) pelagic phytoplankton sterols (brassicasterol and dinosterol), (E) PIP_{25} ($P_{III}IP_{25}$, P_BIP_{25}, and P_DIP_{25}), and (f) terrestrial sterols (campesterol+β-sitosterol). All records are plotted as ka b2k. Yellow bars indicate the GIs (i.e., GI-9 and GI-8) as defined in the NGRIP ice core (Rasmussen et al., 2014). Grey boxes stand for the classification of PIP_{25} values (from darkest to lightest: 0.75–1 extensive sea ice, 0.5–0.75 seasonal ice/stable ice edge, and 0–0.5 reduced ice) (Müller et al., 2011; Xiao et al., 2015; Stein et al., 2017). The black dashed lines represent the divisions between different time periods based on the identified changes in concentrations of all biomarkers and PIP_{25} values (the distribution of IP_{25} and phytoplankton biomarker concentrations refers to Fig. 4).

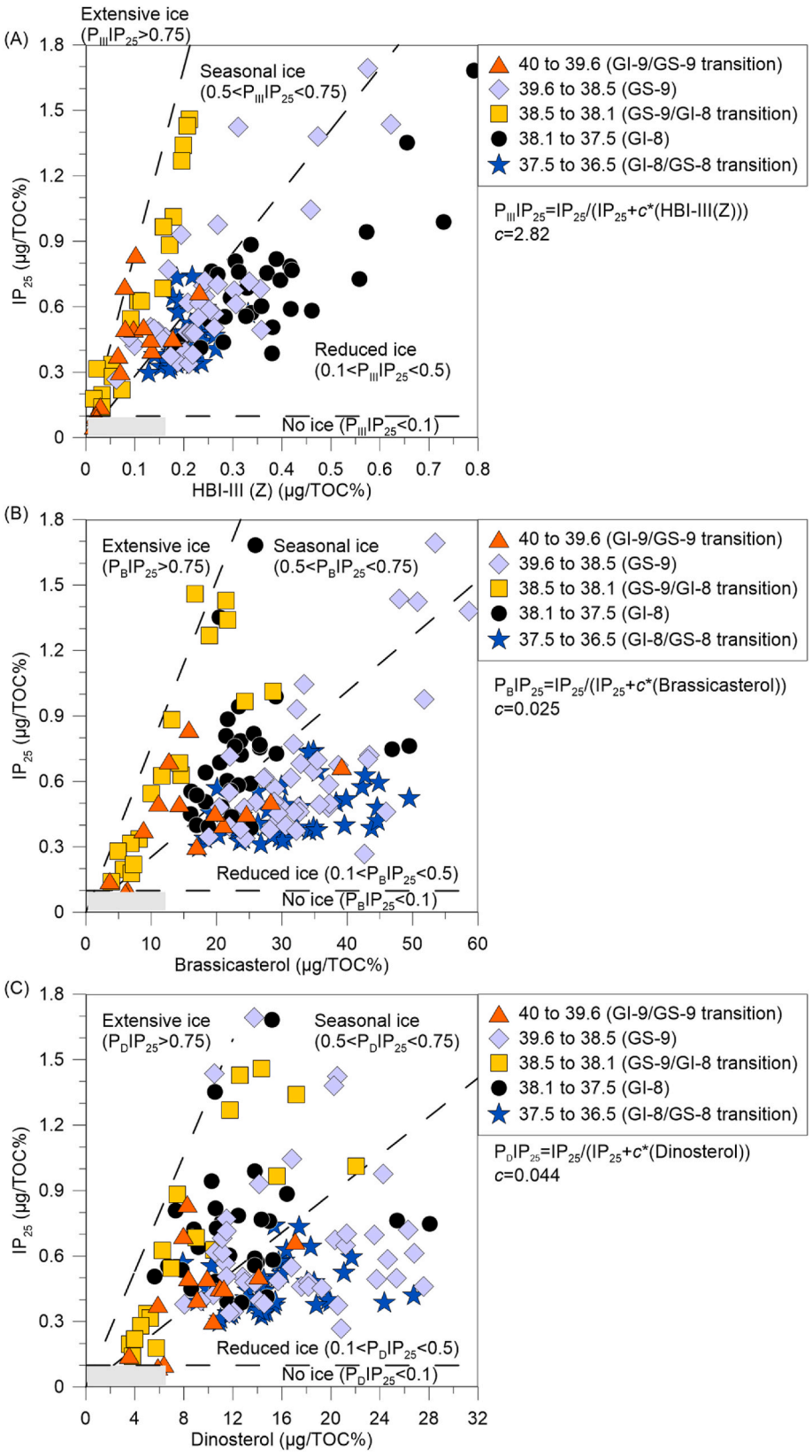

Fig. 4. Cross-plots between IP_{25} and phytoplankton markers, (A) IP_{25} - HBI-III (Z), (B) IP_{25} - brassicasterol, and (C) IP_{25} - dinosterol. The black dashed lines are drawn based on the balance factor *c* from this study, and they represent the differentiation of various sea ice conditions as defined by PIP_{25} (Müller et al., 2011; Xiao et al., 2015; Stein et al., 2017). Different color codes illustrate the results by different time periods.

during this time period (Fig. 3F).

Between 38.1 and 37.5 ka b2k, HBI concentrations were variable, especially between 37.8 and 37.5 ka b2k (Figs. 3C & 4). Brassicasterol and dinosterol concentrations varied throughout this time period (Figs. 3D & 4). Between 38.1 and 37.5 ka b2k, average values for $P_{III}IP_{25}$, P_BIP_{25}, and P_DIP_{25} were 0.4, 0.5, and 0.6, respectively (Fig. 3E). Mean concentration of campesterol+β-sitosterol during this time period was 25.2 μg/TOC% (Fig. 3F).

Between 37.5 and 36.5 ka b2k, HBI concentrations were consistently low, while pelagic phytoplankton sterol concentrations increased and continued to show variability (Figs. 3C, D & 4). Mean PIP_{25} values were 0.4between 37.5 and 36.5 ka b2k (Fig. 3E), and the average concentration of campesterol+β-sitosterol was 29 μg/TOC% (Fig. 3F).

5. Discussion

Through interpretations of our new biomarker-based reconstructions and integrating our results with results from existing studies, we map how the sea ice distribution varied in the Nordic Seas through a D-O oscillation (GS-9 and GI-8). Based on changes in sea ice biomarker concentrations in MD99-2304, the investigated time interval is divided into five time periods: (1) 40–39.6 ka b2k during the GI-9/GS-9 transition, (2) 39.6–38.5 ka b2k during GS-9, (3) 38.5–38.1 ka b2k during the GS-9/GI-8 transition, (4) 38.1–37.5 ka b2k during GI-8, and (5) 37.5–36.5 ka b2k during the GI-8 and GI-8/GS-8 transition (Figs. 3 & 4). For each defined interval we first discuss what our new data tells us about the sea ice conditions in the eastern Fram Strait. Thereafter we consider this new knowledge in the context of existing regional reconstructions and present updated charts of sea ice extent for the five time intervals representing the sea ice changes taking place between 40 and 36.5 ka b2k.

5.1. The GI-9/GS-9 transition (40–39.6 ka b2k): a nearly perennial sea ice cover

Our biomarker results from MD99-2304 show that the eastern Fram Strait was predominantly covered by perennial, or nearly perennial sea ice between 40 and 39.6 ka b2k with limited variability (Figs. 3 & 4). From 40 to 39.8 ka b2k, rapid sea ice expansion occurred, documented by the decreases in HBI and sterol concentrations. At 39.8 ka b2k, the very low HBI and sterol concentrations indicate nearly perennial sea ice. Nevertheless, the PIP_{25} values point to seasonal sea ice at the site, and they contradict our interpretation based on the HBI and sterol records. We argue that the PIP_{25} indices between 40 and 39.8 ka b2k may underestimate what the sea ice condition was like due to the very low concentrations of HBIs and sterols (Figs. 3C, D & E). This argument is supported by previous studies, which showed how the PIP_{25} indices have limitations in areas with permanent sea ice coverage (e.g., Belt et al., 2007; Kim et al., 2019; Kolling et al., 2020). Hence, PIP_{25} values are excluded from the interpretation of sea ice conditions between 40 and 39.8 ka b2k, when we argue that perennial sea ice prevailed. Partly ice-free conditions emerged from 39.8 ka b2k onwards. From 39.8 to 39.6 ka b2k, documented by a temporal resolution of 28 years/sample through this 200-year long time interval, increasing sterol concentrations show that partly ice-free conditions emerged (Figs. 3D & F) (Müller et al., 2011; Xiao et al., 2015; Stein et al., 2017).

Northwest of MD99-2304, the core site of HH15-1252 PC (3 in Fig. 1) was covered by perennial sea ice between 40 and 39.6 ka b2k (El bani Altuna et al., 2024). South of MD99-2304, the Vøring Plateau (MD95-2010, 4 in Fig. 1) was covered by nearly perennial sea ice, and the Faroe-Shetland Channel (MD99-2284, 6 in Fig. 1) was seasonally ice-covered (Sadatzki et al., 2019, 2020). A perennial or nearly perennial sea ice cover also prevailed in the Labrador Sea (GS16-204-23-CC, 7 in Fig. 1) (Scoto et al., 2022). Coupling these with biomarker concentrations and PIP_{25} indices from Core MD99-2304 (Figs. 5 & S1), we propose the presence of nearly perennial sea ice cover in the eastern

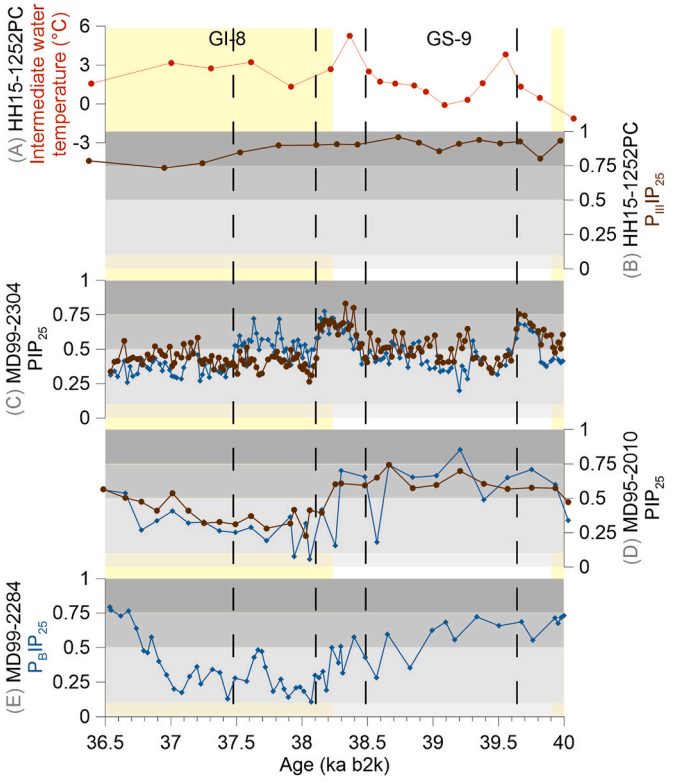

Fig. 5. PIP_{25} indices from MD99-2304 compared to (A) intermediate water temperature and (B) $P_{III}IP_{25}$ from HH15-1252 PC (3 in Fig. 1, El bani Altuna et al., 2024), (C) PIP_{25} from MD99-2304, (D) PIP_{25} from MD95-2010 (4 in Fig. 1, Sadatzki et al., 2020), and (E) P_BIP_{25} from MD99-2284 (6 in Fig. 1, Sadatzki et al., 2019). PIP_{25} indices from PS92/039-2 (1 in Fig. 1, Kremer et al., 2018b) and PS93/006-1 (2 in Fig. 1, Kremer et al., 2018a) were with low temporal resolution during the investigated time interval and hence were excluded from this discussion. Indices from JM11-FI-19PC (5 in Fig. 1, Hoff et al., 2016) were not included here either, since they had a lower temporal resolution compared to those from MD99-2284 and they agreed with the indices from MD99-2284 (Sadatzki et al., 2019). PIP_{25} indices were not calculated in GS16-204-23CC (7 in Fig. 1), due to the in-phase variations in IP_{25} and phytoplankton markers (Scoto et al., 2022). The yellow bars indicate the GIs (i.e., GI-9 and GI-8). The grey boxes at PIP_{25} values refer to extensive sea ice (0.75–1), seasonal ice/stable ice edge (0.5–0.75), and reduced ice (0–0.5) (Xiao et al., 2015; Stein et al., 2017). The brown lines with round symbols refer to $P_{III}IP_{25}$, and the blue lines with oval symbols represent P_BIP_{25}. The black dashed lines represent the five time periods of sea ice change in the eastern Fram Strait.

Fram Strait and a substantial area of the Nordic Seas between 40 and 39.6 ka b2k (Fig. 6A). Such an expanded sea ice extent was likely related to the regional cooling recorded by NGRIP $\delta^{18}O$ (Fig. 3A) (Rasmussen et al., 2014).

5.2. GS-9 (39.6–38.5 ka b2k): polynya activity

Following the nearly perennial sea ice conditions around the GI-9/GS-9 transition (Fig. 6A), seasonal polynyas were active at MD99-2304 between 39.6 and 38.5 ka b2k. From 39.6 ka b2k, all biomarker concentrations stabilized at higher levels (Fig. 3). The combination of elevated HBI and sterol concentrations suggests the occurrence of seasonally ice-free areas in the vicinity of the MIZ, while the constant occurrence of intermediate IP_{25} concentrations shows that sea ice was present at our study site throughout the interval between 39.6 and 38.5 ka b2k (Xiao et al., 2015; Smik et al., 2016; Stein et al., 2017). Between 38.9 and 38.5 ka b2k, the absolute concentrations of all biomarkers increased. This increase is interpreted to reflect reduced sea ice extent

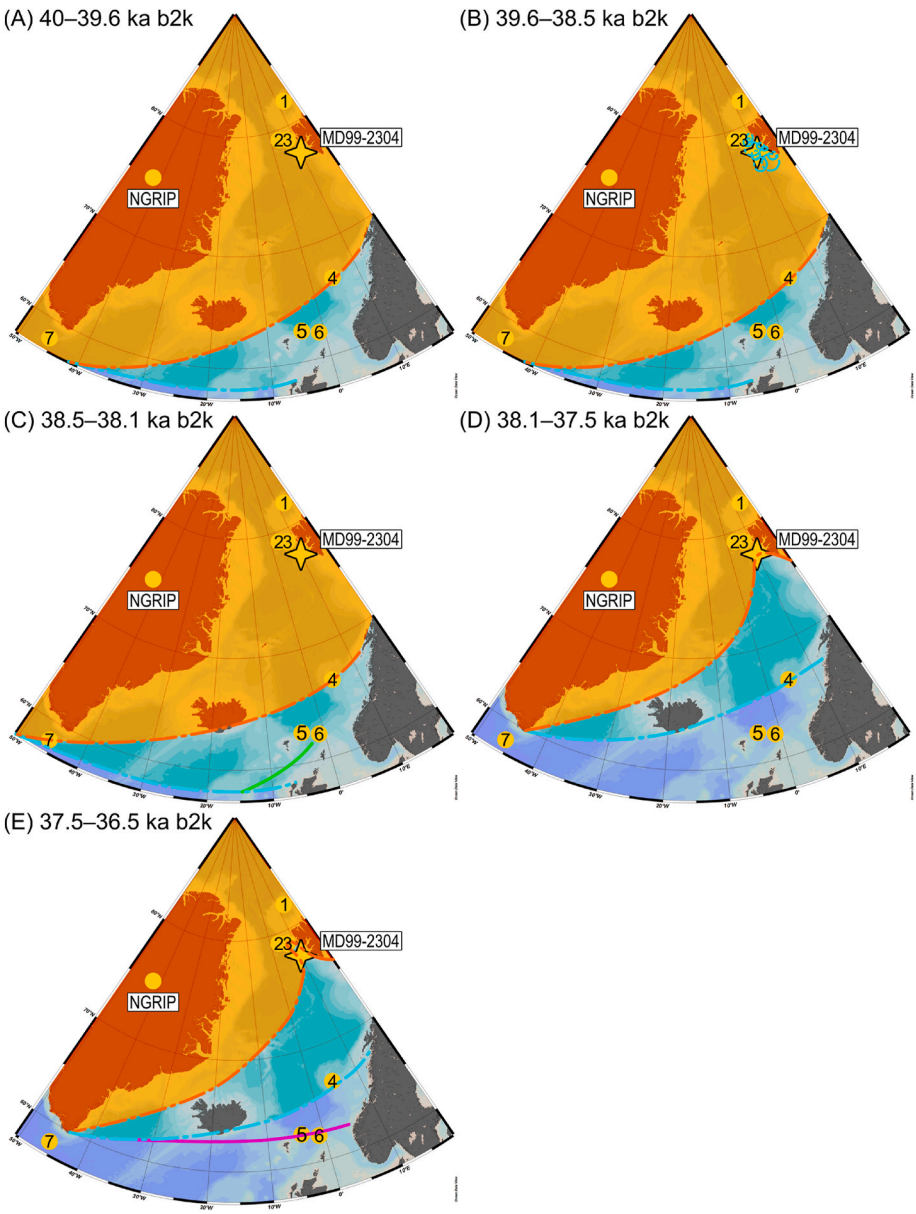

Fig. 6. Schematic sea ice boundaries in the eastern Nordic Seas (A) during the GI-9/GS-9 transition (40–39.6 ka b2k), (B) during GS-9 (39.6–38.5 ka b2k), (C) during the GS-9/GI-8 transition (38.5–38.1 ka b2k), (D) during the first half of GI-8 (38.1–37.5 ka b2k), (E) during the second half of GI-8 and GI-8/GS-8 transition (37.5–36.5 ka b2k). The orange line bounded orange areas represent summer/fall sea ice extent, and the blue line bounded light blue areas indicate winter/spring sea ice extent. The circles with blue dashed lines refer to polynyas. The green line means sea ice retreat during the GS-9/GI-8 transition, and the magenta line characterizes sea ice expansion during the GI-8/GS-8 transition.

(Xiao et al., 2015; Stein et al., 2017).

Our results contrast the established picture of an extensive sea ice cover in the northern Nordic Seas during GSs. Earlier studies have argued for an extensive sea ice cover from further north in the Fram Strait (HH15-1252 PC, El bani Altuna et al., 2024), throughout the western Nordic Seas to the Labrador Sea (GS16-204-23-CC, Scoto et al., 2022). The extensive sea ice cover was also suggested to have reached eastwards to the Vøring Plateau in the Norwegian Sea (Sadatzki et al., 2020). Seasonal sea ice characterized the southeastern Nordic Seas (MD99-2284, Sadatzki et al., 2020). These interpretations are based on the variations in biomarker concentrations and PIP_{25} indices (Figs. 5 & S1). Since we see clear evidence of seasonally ice-free conditions in the eastern Fram Strait at the same time as the surrounding areas were covered by sea ice, we argue for repetitive polynya activity at MD99-2304 between 39.8 and 38.5 ka b2k (Fig. 6B).

Polynyas can be driven by mechanical and/or thermal forces (Morales Maqueda et al., 2004). During the Last Glacial Maximum (LGM), strong easterly katabatic winds likely originated from land and blew off the coast, triggering the formation of coastal polynyas in the Nordic Seas (Knies and Stein, 1998; Knies et al., 2018; Kremer et al., 2018a; El bani Altuna et al., 2021). The Svalbard Barents Sea Ice Sheet (SBIS) played a crucial role in setting up katabatic winds during LGM (Knies et al., 1998; Kremer et al., 2018b), since the formation of katabatic winds is largely buoyancy- and topography-related (Parish and Cassano, 2003; Zammett and Fowler, 2007). MD99-2304 is located close to the glacial SBIS margin. However, the SBIS was likely much smaller during our investigated time interval than during glacial maxima (e.g., Ingólfsson and Landvik, 2013; Jessen and Rasmussen, 2018; Wiberg et al., 2022). The lack of evidence for a large SBIS in the time interval of our study suggests that the polynyas were not formed due to the existence of strong katabatic winds.

Rather, we suggest that the polynyas documented at MD99-2304

emerged as a response to changes in the oceanic sensible heat flux. During the cold GSs, the Nordic Seas were strongly stratified (Dokken et al., 2013; Wary et al., 2015). Warm and saline AW submerged below the sea ice and the cold, fresh halocline before reaching the MIZ. The cold, fresh surface layer which consisted mostly of sea ice prevented heat release from the AW to the atmosphere, and a heat reservoir that spanned the full Nordic Seas built up at intermediate water depths (Sessford et al., 2019; El bani Altuna et al., 2021). As the heat reservoir built up at the onset of GS-9 (El bani Altuna et al., 2021), local mixing could be initiated by upward fluxes of heat and salt that weakened the halocline and facilitated the formation of open water polynyas (Rheinlænder et al., 2021). Sea ice has been shown to be highly sensitive to changes in subsurface AW temperatures (Jensen et al., 2016). Lower water temperature at intermediate depths is seen at the Fram Strait site HH15-1252 PC during the interval where we argue for polynya activity (Figs. 3 & 5A), since ocean heat may have been released through these local polynyas. Sensible heat polynyas could also be sustained through upwelling of subsurface AW along the shelf break of western Svalbard (Morales Maqueda et al., 2004; Falk-Petersen et al., 2015). In brief, we consider oceanic sensible heat the most likely driver of polynya formation at MD99-2304 between 39.8 and 38.5 ka b2k.

5.3. The GS-9/GI-8 transition (38.5–38.1 ka b2k): a nearly perennial sea ice cover

Just prior to the GS-9/GI-8 transition, a nearly perennial sea ice cover prevailed in the eastern Fram Strait, followed by a gradual decrease in regional sea ice extent towards the onset of GI-8. Between 38.5 and 38.3 ka b2k, all biomarkers dropped to very low concentrations that were only observed between 39.9 and 39.7 ka b2k (Fig. 3), suggesting low primary productivity and little terrestrial organic matter deposition. Such conditions reflect a lasting, nearly perennial sea ice cover at the site (Xiao et al., 2013, 2015; Stein et al., 2017; Kolling et al., 2020). Due to the very low HBI concentrations, we suggest that the PIP_{25} values that indicate a seasonal sea ice coverage may underestimate the sea ice conditions at the site between 38.5 and 38.3 ka b2k, in the same way as for the HBI concentration minimum at 39.8 ka b2k (Fig. 3C, D & E). Between 38.3 and 38.1 ka b2k, increasing biomarker concentrations, both for the HBIs and sterols, imply a progressive reduction in sea ice extent, from perennial to seasonal (Fig. 3) (Stein et al., 2017; Kolling et al., 2020).

The regrowth to a nearly perennial sea ice cover at the site between 38.5 and 38.1 ka b2k can be seen as a response to a depletion of the ocean heat reservoir. The polynyas that were active throughout the 39.8–38.5 ka b2k time interval allowed for continuous local ocean heat loss to the atmosphere (Maykut, 1982). Once the ocean heat reservoir was depleted, sea ice could regrow and the halocline could be established again within a short time (Rheinlænder et al., 2021), as observed in our record. The intermediate water temperature reconstruction of HH15-1252 PC further supports this scenario. Lower temperatures are recorded in the interval with polynya activity, and higher temperatures are recorded when the sea ice cover is interpreted to have been nearly perennial, reflecting whether heat could be released from the ocean (Fig. 5A) (El bani Altuna et al., 2021).

In line with our findings, El bani Altuna et al. (2024)suggested a perennial sea ice cover at HH15-1252 PC between 38.5 and 38.1 ka b1k. In the southeastern Nordic Seas, sea ice almost disappeared from the Faroe-Shetland Channel (MD99-2284) during this time period, while seasonal sea ice was still present at the Vøring Plateau (MD95-2010) until 38.3 ka b2k. These southern regions were mostly ice-free after the GS-9/GI-8 transition at 38.22 ka b2k (Sadatzki et al., 2019, 2020). In the Labrador Sea, the sea ice retreated to a seasonal extent after the GS-9/GI-8 transition, as shown by the increase in HBIs and brassicasterol concentrations (Scoto et al., 2022) (Fig. S1). Although seasonally ice-free areas gradually reached MD99-2304 between 38.3 and 38.1 ka b2k (Fig. 6C), the duration of seasonal sea ice retreat was likely shorter, and seasonally ice-free conditions occurred less frequently in the eastern Fram Strait when compared to the southeastern Nordic Seas sites (MD99-2284 and MD95-2010) (Figs. 5 & S1) (Sadatzki et al., 2019, 2020).

5.4. GI-8 (38.1–37.5 ka b2k): a seasonal sea ice margin

The combined interpretation, incorporating both PIP_{25} values and biomarker concentrations, suggests a changeable environment characterized by seasonal sea ice and occasionally limited ice at MD99-2304 between 38.1 and 37.5 ka b2k (Fig. 3) (Müller et al., 2011; Xiao et al., 2015; Stein et al., 2017).

At the same time, a seasonal ice cover prevailed at HH15-1252 PC, north of MD99-2304 (El bani Altuna et al., 2024). Further south, the sea ice edge reached the Vøring Plateau (MD95-2010) during winter/spring, and the Faroe-Shetland Channel (MD99-2284) was mostly ice-free all year round (Sadatzki et al., 2019, 2020). Sea ice also gradually retreated from the Labrador Sea (GS16-204-23-CC) during this time period (Scoto et al., 2022). Seeing our biomarker and PIP_{25} results from MD99-2304 in the context of these regional sea ice reconstructions (Figs. 5 & S1), we argue that the summer/fall sea ice edge was located close to MD99-2304 between 38.1 and 37.5 ka b2k (Fig. 6D) (Belt et al., 2015; Stein et al., 2017; Kolling et al., 2020).

As the sea ice extent began to retreat northward, warm and saline AW reached the surface of the southeastern Nordic Seas (Sadatzki et al., 2019, 2020). During this period, the atmosphere in the Nordic Seas received a greater amount of heat and moisture, in comparison to when the sea surface was predominantly covered by sea ice (i.e., during the GSs). This release of heat may have contributed to regional warming (Hoff et al., 2016; Sadatzki et al., 2020; El bani Altuna et al., 2021). Sea ice retreat in the Arctic Mediterranean also contributed to changes in near-surface wind, in the form of e.g. acceleration and redirection (Mioduszewski et al., 2018; Ogawa and Spengler, 2019; Liu et al., 2024). Together, the release of ocean heat and changes in wind field may further have accelerated the seasonal opening along the eastern Nordic Seas to the eastern Fram Strait (Hoff et al., 2016; Alkama et al., 2020).

5.5. The GI-8 and GI-8/GS-8 transition (37.5–36.5 ka b2k): seasonally ice-free condition

Between 37.5 and 36.5 ka b2k, the eastern Fram Strait was covered by seasonal sea ice, and the summer/fall sea ice edge moved north of MD99-2304. HBIs were present in MD99-2304, however, their concentrations remained low (Fig. 3C). The increases in sterol concentrations imply a retreating sea ice cover and larger areas with open ocean (Fig. 3D and F) (Volkman, 2006; Kolling et al., 2020). PIP_{25} values indicate a limited extent of sea ice at MD99-2304 (Figs. 3E & 4) (Xiao et al., 2015; Stein et al., 2017).

The summer/fall sea ice edge was frequently positioned in the vicinity of HH15-1252 PC until 37 ka b2k, when the sea ice extent started to increase (El bani Altuna et al., 2024). South of the Fram Strait, the Nordic Seas were largely ice-free until 36.9 ka b2k. From 36.9 ka b2k, the winter/spring sea ice gradually expanded towards the Vøring Plateau (MD95-2010) and the Faroe-Shetland Channel (MD99-2284) (Sadatzki et al., 2019, 2020). In the Labrador Sea, the sea ice cover started to grow from 36.7 ka b2k (Scoto et al., 2022). Integrating the biomarker and PIP_{25} results from our new and these existing records (Fig. 5 & S1), we argue that the summer/fall sea ice edge was located close to HH15-1252 PC between 37.5 and 36.5 ka b2k, while MD99-2304 was free of sea ice during summers (Fig. 6E).

5.6. Climate implications

Changes in the sea ice extent are proposed to regulate the millennial-scale climate changes during the last glacial (e.g., Jensen et al., 2016; Menviel et al., 2020; Sadatzki et al., 2020; El bani Altuna et al., 2024).

During the end of GI-9 and the onset of GS-9, the Nordic Seas were covered by sea ice from the Greenland-Scotland Ridge to the Fram Strait (this study; Sadatzki et al., 2019, 2020; Scoto et al., 2022; El bani Altuna et al., 2024). With such an extensive sea ice cover, enhanced regional cooling is expected due to the ice-albedo feedback and restricted release of ocean heat to the atmosphere (Dokken et al., 2013; Li and Born, 2019; Malmierca-Vallet and Sime, 2023). The relation between sea ice expansion and regional cooling is further supported by the correlation between cooling reflected in the NGRIP $\delta^{18}O$ and $\delta^{15}N$ temperature reconstructions (Kindler et al., 2014; Rasmussen et al., 2014) and the observed sea ice expansion in the eastern Nordic Sea records during the GI-9/GS-9 transition (this study; Sadatzki et al., 2019, 2020).

The polynya activity in the eastern Fram Strait during GS-9 can alter the amount of absorbed radiation via the albedo effect (Morales Maqueda et al., 2004), and facilitate heat and moisture exchange between the ocean and the atmosphere (Maykut, 1982; Haid and Timmermann, 2013). Depending on the size of the polynyas, enough moisture could be provided to feed onshore ice sheets (e.g., Hebbeln et al., 1994; Li et al., 2010; Simon et al., 2023). However, the impact of this oceanic heat and moisture release on climate was likely confined to a local scale near Svalbard, since the polynya activity was local and possibly had a limited spatial extension. No detailed reconstructions are available regarding the extension of the SBIS during the investigated time interval, but existing knowledge on the SBIS extent (e.g., Ingólfsson and Landvik, 2013; Jessen and Rasmussen, 2018; Wiberg et al., 2022) does not support significant growth of the ice sheet as a response to the polynyas. Neither are there any indications in the NGRIP $\delta^{18}O$ record (Fig. 3A), although this may be expected, as the hydrological cycle of Greenland is likely to separate from the Fram Strait (Charles et al., 1994; Masson-Delmotte et al., 2005; Guillevic et al., 2014).

Furthermore, recurrent polynyas can induce ocean convection to a limited depth, destabilizing the halocline. This is primarily due to the densification of the surface water as a response to oceanic heat loss through the polynyas (Fig. 5A) (Backhaus et al., 1997; Goosse and Fichefet, 2001; Rheinlænder et al., 2021).

Just before the GS-9/GI-8 transition at 38.22 ka b2k, when a nearly perennial sea ice cover occupied large parts of the Nordic Seas, the effect of the reduced heat release from the ocean to the atmosphere is reflected by increased intermediate water temperatures (Sessford et al., 2019; El bani Altuna et al., 2021). However, as soon as the sea ice cover retreated northwards around the GS-9/GI-8 transition, the excess ocean heat was released into the atmosphere. This released heat may have played a significant role in the recorded temperature overshoot observed in the NGRIP $\delta^{18}O$ after the GS-9/GI-8 transition (Fig. 3A) (Hoff et al., 2016; Sadatzki et al., 2019).

During GI-8, when there was a seasonal sea ice cover in the eastern Nordic Seas, the sea surface albedo was reduced. A reduced sea ice cover with more ice-free areas could facilitate the transport of ocean heat to higher latitudes and allow for heat release to the atmosphere as the AW flows northwards (Smedsrud et al., 2022). The release of ocean heat has significant implications for regional and even global climate, including effects on ocean convection, NADW formation, and AMOC stability (Dokken et al., 2013; Li and Born, 2019; Sadatzki et al., 2020; Malmierca-Vallet and Sime, 2023). Additionally, enhanced moisture from the ice-free sea surface may be advected towards land and precipitation would increase, potentially influencing the size of the Fennoscandian Ice Sheet and SBIS (e.g. as described in Simon et al., 2023). The changing ice sheets would, in turn, control regional and global climate oscillations. When ice sheets grow, they can influence surface albedo and atmospheric CO_2 level, leading to changes in Earth's energy budget and cooling in the climate system (e.g., Zeng, 2003; Stap et al., 2014; Wadham et al., 2019). Moreover, the elevated ice sheets can affect wind direction and strength and further have an impact on AMOC and global heat redistribution (e.g., Sherriff-Tadano et al., 2018; Li and Born, 2019). In the North Atlantic and Nordic Seas, freshwater flux controlled by ice sheet instability is associated with changes in NADW formation and thus large-scale climate oscillations (e.g., Mignot et al., 2007; Roche et al., 2010; Li et al., 2024).

6. Conclusions

Our new biomarker records from the eastern Fram Strait document the occurrence of open water conditions in the form of polynyas during GS-9, contrasting previous understanding of GS sea ice conditions in this area. During the transition into GI-8, the perennial sea ice cover disappeared later than further south in the eastern Nordic Seas. GI-8 is characterized by the occurrence of seasonal sea ice at MD99-2304.

By integrating our new results with previously published biomarker-based sea ice reconstructions from the North Atlantic and the Nordic Seas, updated sea ice charts are presented. Between 40 and 39.6 ka b2k (during the GI-9/GS-9 transition), extensive sea ice dominated the Nordic Seas, with the winter/spring sea ice edge reaching south of the Erik Drift and the Faroe-Shetland Channel. The summer/fall sea ice retreated towards the Vøring Plateau.

During GS-9, between 39.6 and 38.5 ka b2k, the southern location of the sea ice extent was comparable to the preceding period. However, in the eastern Fram Strait, repetitive polynya activity took place.

The polynyas were closed from 38.5 ka b2k, corresponding to when the sea ice edge started to retreat from the Erik Drift and the Faroe-Shetland Channel.

The GI-8 winter/spring sea ice retreated to just north of the Eirik Drift and in the Nordic Seas to the Vøring Plateau. During summer/fall, the eastern part of the North Atlantic and Nordic Seas sea ice cover retreated northwards to the eastern Fram Strait. In the later part of GI-8, 37.5–36.5 ka b2k, the summer/fall sea ice edge was located just north of MD99-2304.

CRediT authorship contribution statement

Wanyee Wong: Conceptualization, Methodology, Validation, Formal analysis, Investigation, Data Curation, Writing – original draft, Writing – review & editing, Visualization. **Bjørg Risebrobakken:** Conceptualization, Investigation, Resources, Writing – original draft, Writing – review & editing, Visualization, Supervision, Project administration, Funding acquisition. **Kirsten Fahl:** Methodology, Validation, Resources, Data Curation, Writing – review & editing, Supervision. **Ruediger Stein:** Methodology, Formal analysis, Investigation, Writing – review & editing, Visualization, Supervision. **Eystein Jansen:** Investigation, Writing – review & editing, Supervision. **Kristine Steinsland:** Investigation, Writing – review & editing, Visualization. **Catherine Kissel:** Methodology, Validation, Resources, Writing – review & editing.

Declaration of competing interest

The authors declare that they have no known competing financial interests or personal relationships that could have appeared to influence the work reported in this paper.

Data availability

For MD99-2304, biomarker data is available from https://doi.org/10.1594/PANGAEA.971113 and magnetic susceptibility from https://doi.org/10.1594/PANGAEA.971511. Magnetic susceptibility of MD99-2284 is available from https://doi.pangaea.de/10.1594/PANGAEA.971542. The updated biomarker dataset of MD95-2010 is available from https://doi.org/10.1594/PANGAEA.971530.

Acknowledgement

We would like to thank the crew of cruise Marion Dufresne IMAGES 5 1999 for retrieving Core MD99-2304 on leg MD114, Defang You of Alfred Wegener Institute (AWI) for assisting with the biomarker

measurements and fruitful discussions, Malin Ödalen of Norwegian Research Centre (NORCE) for the valuable comments, Walter Luttmer of AWI for assisting the biomarker and TOC measurements, Valéa Schumacher, Frederike Schmidtand, Anja Müller, Amelie Nübel, Jens Strauss, and Justin Lindemann of AWI for assisting the TOC measurements and analytical discussion of TOC measurement techniques. This research is funded by the Research Council of Norway (RCN) funded project ABRUPT Arctic Climate Change (project number 325333).

Appendix A. Supplementary data

Supplementary data to this article can be found online at https://doi.org/10.1016/j.quascirev.2024.108916.

References

Alkama, R., Koffi, E.N., Vavrus, S.J., Diehl, T., Francis, J.A., Stroeve, J., Forzieri, G., Vihma, T., Cescatti, A., 2020. Wind amplifies the polar sea ice retreat. Environ. Res. Lett. 15, 124022 https://doi.org/10.1088/1748-9326/abc379.

Andersen, K.K., Svensson, A., Johnsen, S.J., Rasmussen, S.O., Bigler, M., Röthlisberger, R., Ruth, U., Siggaard-Andersen, M.L., Peder Steffensen, J., Dahl-Jensen, D., Vinther, B.M., Clausen, H.B., 2006. The Greenland Ice Core Chronology 2005, 15-42 ka. Part 1: constructing the time scale. Quat. Sci. Rev. 25, 3246–3257. https://doi.org/10.1016/j.quascirev.2006.08.002.

Backhaus, J.O., Fohrmann, H., Kämpf, J., Rubino, A., 1997. Formation and export of water masses produced in Arctic shelf polynyas — process studies of oceanic convection. ICES J. Mar. Sci. 54, 366–382. https://doi.org/10.1006/jmsc.1997.0230.

Barber, D.G., Massom, R.A., 2007. The Role of Sea Ice in Arctic and Antarctic Polynyas, pp. 1–54. https://doi.org/10.1016/S0422-9894(06)74001-6.

Belt, S.T., Allard, W.G., Massé, G., Robert, J.-M., Rowland, S.J., 2000. Highly branched isoprenoids (HBIs): identification of the most common and abundant sedimentary isomers. Geochim Cosmochim Acta 64, 3839–3851. https://doi.org/10.1016/S0016-7037(00)00464-6.

Belt, S.T., Cabedo-Sanz, P., Smik, L., Navarro-Rodriguez, A., Berben, S.M.P., Knies, J., Husum, K., 2015. Identification of paleo Arctic winter sea ice limits and the marginal ice zone: optimised biomarker-based reconstructions of late Quaternary Arctic sea ice. Earth Planet Sci. Lett. 431, 127–139. https://doi.org/10.1016/j.epsl.2015.09.020.

Belt, S.T., Massé, G., Rowland, S.J., Poulin, M., Michel, C., LeBlanc, B., 2007. A novel chemical fossil of palaeo sea ice: IP25. Org. Geochem. 38, 16–27. https://doi.org/10.1016/j.orggeochem.2006.09.013.

Bennett, M.G., Renfrew, I.A., Stevens, D.P., Moore, G.W.K., 2024. The Northeast water polynya, Greenland: climatology, atmospheric forcing and ocean response. J Geophys Res Oceans 129. https://doi.org/10.1029/2023JC020513.

Berben, S.M.P., Dokken, T.M., Abbott, P.M., Cook, E., Sadatzki, H., Simon, M.H., Jansen, E., 2020. Independent tephrochronological evidence for rapid and synchronous oceanic and atmospheric temperature rises over the Greenland stadial-interstadial transitions between ca. 32 and 40 ka b2k. Quat. Sci. Rev. 236 https://doi.org/10.1016/j.quascirev.2020.106277.

Bianchi, T.S., Canuel, E.A., 2011. Chemical Biomarkers in Aquatic Ecosystems. Princeton University Press. https://doi.org/10.1515/9781400839100.

Boon, J.J., Rijpstra, W.I.C., de Lange, F., de Leeuw, J.W., Yoshioka, M., Shimizu, Y., 1979. Black Sea sterol—a molecular fossil for dinoflagellate blooms. Nature 277, 125–127. https://doi.org/10.1038/277125a0.

Bosse, A., Fer, I., Søiland, H., Rossby, T., 2018. Atlantic water transformation along its poleward pathway across the nordic seas. J Geophys Res Oceans 123, 6428–6448. https://doi.org/10.1029/2018JC014147.

Brown, T.A., Belt, S.T., Tatarek, A., Mundy, C.J., 2014. Source identification of the Arctic sea ice proxy IP 25. Nat. Commun. 5 https://doi.org/10.1038/ncomms5197.

Charles, C.D., Rind, D., Jouzel, J., Koster, R.D., Fairbanks, R.G., 1994. Glacial-Interglacial changes in moisture sources for Greenland: influences on the ice core record of climate. Science 263, 508–511. https://doi.org/10.1126/science.263.5146.508, 1979.

Dokken, T.M., Jansen, E., 1999. Rapid changes in the mechanism of ocean convection during the last glacial period. Nature 401, 458–461. https://doi.org/10.1038/46753.

Dokken, T.M., Nisancioglu, K.H., Li, C., Battisti, D.S., Kissel, C., 2013. Dansgaard-Oeschger cycles: interactions between ocean and sea ice intrinsic to the Nordic seas. Paleoceanography 28, 491–502. https://doi.org/10.1002/palo.20042.

Dörr, J., Årthun, M., Eldevik, T., Sandø, A.B., 2024. Expanding influence of atlantic and pacific ocean heat transport on winter sea-ice variability in a warming arctic. J Geophys Res Oceans 129. https://doi.org/10.1029/2023JC019900.

Dumont, D., 2022. Marginal ice zone dynamics: history, definitions and research perspectives. Phil. Trans. Math. Phys. Eng. Sci. 380 https://doi.org/10.1098/rsta.2021.0253.

El bani Altuna, N., Ezat, M.M., Greaves, M., Rasmussen, T.L., 2021. Millennial-scale changes in bottom water temperature and water mass exchange through the Fram Strait 79°N, 63-13 ka. Paleoceanogr. Paleoclimatol. 36 https://doi.org/10.1029/2020PA004061.

El bani Altuna, N., Ezat, M.M., Smik, L., Muschitiello, F., Belt, S.T., Knies, J., Rasmussen, T.L., 2024. Sea ice-ocean coupling during heinrich stadials in the Atlantic–Arctic gateway. Sci. Rep. 14, 1065. https://doi.org/10.1038/s41598-024-51532-7.

Ezat, M.M., Rasmussen, T.L., Groeneveld, J., 2014. Persistent intermediate water warming during cold stadials in the southeastern Nordic seas during the past 65 k.y. Geology 42, 663–666. https://doi.org/10.1130/G35579.1.

Fahl, K., Stein, R., 2012. Modern seasonal variability and deglacial/Holocene change of central Arctic Ocean sea-ice cover: new insights from biomarker proxy records. Earth Planet Sci. Lett. 351–352, 123–133. https://doi.org/10.1016/j.epsl.2012.07.009.

Fahl, K., Stein, R., 2007. Biomarker records, organic carbon accumulation, and river discharge in the Holocene southern Kara Sea (Arctic Ocean). Geo Mar. Lett. 27, 13–25. https://doi.org/10.1007/s00367-006-0049-8.

Falk-Petersen, S., Pavlov, V., Berge, J., Cottier, F., Kovacs, K.M., Lydersen, C., 2015. At the rainbow's end: high productivity fueled by winter upwelling along an Arctic shelf. Polar Biol. 38, 5–11. https://doi.org/10.1007/s00300-014-1482-1.

Florence, F., Walt, M., Matt, S., Ann, W., 2017. Sea Ice Index, Version 3. National Snow and Ice Data Center.

Gao, Y., Sun, J., Li, F., He, S., Sandven, S., Yan, Q., Zhang, Z., Lohmann, K., Keenlyside, N., Furevik, T., Suo, L., 2015. Arctic sea ice and Eurasian climate: a review. Adv. Atmos. Sci. 32, 92–114. https://doi.org/10.1007/s00376-014-0009-6.

Goosse, H., Fichefet, T., 2001. Open-ocean convection and polynya formation in a large-scale ice–ocean model. Tellus Dyn. Meteorol. Oceanogr. 53, 94. https://doi.org/10.3402/tellusa.v53i1.12175.

Guillevic, M., Bazin, L., Landais, A., Stowasser, C., Masson-Delmotte, V., Blunier, T., Eynaud, F., Falourd, S., Michel, E., Minster, B., Popp, T., Prié, F., Vinther, B.M., 2014. Evidence for a three-phase sequence during Heinrich Stadial 4 using a multiproxy approach based on Greenland ice core records. Clim. Past 10, 2115–2133. https://doi.org/10.5194/cp-10-2115-2014.

Haid, V., Timmermann, R., 2013. Simulated heat flux and sea ice production at coastal polynyas in the southwestern Weddell Sea. J Geophys Res Oceans 118, 2640–2652. https://doi.org/10.1002/jgrc.20133.

Hattermann, T., Isachsen, P.E., von Appen, W.J., Albretsen, J., Sundfjord, A., 2016. Eddy-driven recirculation of Atlantic water in Fram Strait. Geophys. Res. Lett. 43, 3406–3414. https://doi.org/10.1002/2016GL068323.

Hebbeln, D., Dokken, T., Andersen, E.S., Hald, M., Elverhøi, A., 1994. Moisture supply for northern ice-sheet growth during the Last Glacial Maximum. Nature 370, 357–360. https://doi.org/10.1038/370357a0.

Henry, L.G., McManus, J.F., Curry, W.B., Roberts, N.L., Piotrowski, A.M., Keigwin, L.D., 2016. North Atlantic ocean circulation and abrupt climate change during the last glaciation. Science 353. https://doi.org/10.1126/science.aaf5529, 1979.

Hoff, U., Rasmussen, T.L., Stein, R., Ezat, M.M., Fahl, K., 2016. Sea ice and millennial-scale climate variability in the Nordic seas 90 kyr ago to present. Nat. Commun. 7 https://doi.org/10.1038/ncomms12247.

Ingólfsson, Ó., Landvik, J.Y., 2013. The Svalbard–Barents Sea ice-sheet – historical, current and future perspectives. Quat. Sci. Rev. 64, 33–60. https://doi.org/10.1016/j.quascirev.2012.11.034.

Jahn, A., Holland, M.M., Kay, J.E., 2024. Projections of an ice-free Arctic Ocean. Nat. Rev. Earth Environ. https://doi.org/10.1038/s43017-023-00515-9.

Jansen, E., Christensen, J.H., Dokken, T., Nisancioglu, K.H., Vinther, B.M., Capron, E., Guo, C., Jensen, M.F., Langen, P.L., Pedersen, R.A., Yang, S., Bentsen, M., Kjær, H.A., Sadatzki, H., Sessford, E., Stendel, M., 2020. Past perspectives on the present era of abrupt Arctic climate change. Nat. Clim. Change 10, 714–721. https://doi.org/10.1038/s41558-020-0860-7.

Jensen, M.F., Nilsson, J., Nisancioglu, K.H., 2016. The interaction between sea ice and salinity-dominated ocean circulation: implications for halocline stability and rapid changes of sea ice cover. Clim. Dynam. 47, 3301–3317. https://doi.org/10.1007/s00382-016-3027-5.

Jessen, S.P., Rasmussen, T.L., 2018. Ice-rafting patterns on the western Svalbard slope 74-0 ka: interplay between ice-sheet activity, climate and ocean circulation. Boreas. https://doi.org/10.1111/bor.

Kim, J.-H., Gal, J.-K., Jun, S.-Y., Smik, L., Kim, D., Belt, S.T., Park, K., Shin, K.-H., Nam, S.-I., 2019. Reconstructing spring sea ice concentration in the Chukchi Sea over recent centuries: insights into the application of the PIP25 index. Environ. Res. Lett. 14, 125004 https://doi.org/10.1088/1748-9326/ab4b6e.

Kindler, P., Guillevic, M., Baumgartner, M., Schwander, J., Landais, A., Leuenberger, M., 2014. Temperature reconstruction from 10 to 120 kyr b2k from the NGRIP ice core. Clim. Past 10, 887–902. https://doi.org/10.5194/cp-10-887-2014.

Kissel, C., Laj, C., Labeyrie, L., Dokken, T., Voelker, A., Blamart, D., 1999. Rapid climatic variations during marine isotopic stage 3: magnetic analysis of sediments from Nordic Seas and North Atlantic. Earth Planet Sci. Lett. 171, 489–502. https://doi.org/10.1016/S0012-821X(99)00162-4.

Knies, J., Köseoğlu, D., Rise, L., Baeten, N., Bellec, V.K., Bøe, R., Klug, M., Panieri, G., Jernas, P.E., Belt, S.T., 2018. Nordic Seas polynyas and their role in preconditioning marine productivity during the Last Glacial Maximum. Nat. Commun. 9 https://doi.org/10.1038/s41467-018-06252-8.

Knies, J., Stein, R., 1998. New aspects of organic carbon deposition and its paleoceanographic implications along the Northern Barents Sea Margin during the last 30,000 years. Paleoceanography 13, 384–394. https://doi.org/10.1029/98PA01501.

Knies, J., Vogt, C., Stein, R., 1998. Late Quaternary growth and decay of the Svalbard/Barents Sea ice sheet and paleoceanographic evolution in the adjacent Arctic Ocean. Geo Mar. Lett. 18, 195–202. https://doi.org/10.1007/s003670050068.

Kolling, H.M., Stein, R., Fahl, K., Sadatzki, H., de Vernal, A., Xiao, X., 2020. Biomarker distributions in (Sub)-Arctic surface sediments and their potential for Sea Ice reconstructions. G-cubed 21. https://doi.org/10.1029/2019GC008629.

Kremer, A., Stein, R., Fahl, K., Bauch, H., Mackensen, A., Niessen, F., 2018a. A 190-ka biomarker record revealing interactions between sea ice, Atlantic Water inflow and ice sheet activity in eastern Fram Strait. arktos 4, 1–17. https://doi.org/10.1007/s41063-018-0052-0.

Kremer, A., Stein, R., Fahl, K., Ji, Z., Yang, Z., Wiers, S., Matthiessen, J., Forwick, M., Löwemark, L., O'Regan, M., Chen, J., Snowball, I., 2018b. Changes in sea ice cover and ice sheet extent at the Yermak Plateau during the last 160 ka – reconstructions from biomarker records. Quat. Sci. Rev. 182, 93–108. https://doi.org/10.1016/j.quascirev.2017.12.016.

Li, C., Battisti, D.S., Bitz, C.M., 2010. Can North Atlantic sea ice anomalies account for Dansgaard-Oeschger climate signals? J. Clim. 23, 5457–5475. https://doi.org/10.1175/2010JCLI3409.1.

Li, C., Born, A., 2019. Coupled atmosphere-ice-ocean dynamics in Dansgaard-Oeschger events. Quat. Sci. Rev. https://doi.org/10.1016/j.quascirev.2018.10.031.

Li, D., DeConto, R.M., Pollard, D., Hu, Y., 2024. Competing climate feedbacks of ice sheet freshwater discharge in a warming world. Nat. Commun. 15, 5178. https://doi.org/10.1038/s41467-024-49604-3.

Liu, W., Yang, S., Chen, D., Zha, J., Zhang, G., Zhang, Z., Zhang, T., Xu, L., Hu, X., Deng, K., 2024. Rapid acceleration of arctic near-surface wind speed in a warming climate. Geophys. Res. Lett. 51 https://doi.org/10.1029/2024GL109385.

Malmierca-Vallet, I., Sime, L.C., 2023. Dansgaard–Oeschger events in climate models: review and baseline Marine Isotope Stage 3 (MIS3) protocol. Clim. Past 19, 915–942. https://doi.org/10.5194/cp-19-915-2023.

Masson-Delmotte, V., Jouzel, J., Landais, A., Stievenard, M., Johnsen, S.J., White, J.W.C., Werner, M., Sveinbjornsdottir, A., Fuhrer, K., 2005. GRIP deuterium excess reveals rapid and orbital-scale changes in Greenland moisture origin. Science 309, 118–121. https://doi.org/10.1126/science.1108575, 1979.

Maykut, G.A., 1982. Large-scale heat exchange and ice production in the central Arctic. J. Geophys. Res. 87, 7971–7984. https://doi.org/10.1029/JC087iC10p07971.

McManus, J.F., Oppo, D.W., Cullen, J.L., 1999. A 0.5-million-year record of millennial-scale climate variability in the North Atlantic. Science 283, 971–975. https://doi.org/10.1126/science.283.5404.971, 1979.

Menviel, L.C., Skinner, L.C., Tarasov, L., Tzedakis, P.C., 2020. An ice–climate oscillatory framework for Dansgaard–Oeschger cycles. Nat. Rev. Earth Environ. https://doi.org/10.1038/s43017-020-00106-y.

Mignot, J., Ganopolski, A., Levermann, A., 2007. Atlantic subsurface temperatures: response to a shutdown of the overturning circulation and consequences for its recovery. J. Clim. 20 (1), 4884–4898. https://doi.org/10.1175/JCLI4280.

Mioduszewski, J., Vavrus, S., Wang, M., 2018. Diminishing arctic Sea Ice promotes stronger surface winds. J. Clim. 31, 8101–8119. https://doi.org/10.1175/JCLI-D-18-0109.1.

Morales Maqueda, M.A., Willmott, A.J., Biggs, N.R.T., 2004. Polynya dynamics: a review of observations and modeling. Rev. Geophys. 42 https://doi.org/10.1029/2002RG000116.

Muilwijk, M., Smedsrud, L.H., Ilicak, M., Drange, H., 2018. Atlantic water heat transport variability in the 20th century Arctic Ocean from a global ocean model and observations. J Geophys Res Oceans 123, 8159–8179. https://doi.org/10.1029/2018JC014327.

Müller, J., Massé, G., Stein, R., Belt, S.T., 2009. Variability of sea-ice conditions in the Fram Strait over the past 30,000 years. Nat. Geosci. 2, 772–776. https://doi.org/10.1038/ngeo665.

Müller, J., Wagner, A., Fahl, K., Stein, R., Prange, M., Lohmann, G., 2011. Towards quantitative sea ice reconstructions in the northern North Atlantic: a combined biomarker and numerical modelling approach. Earth Planet Sci. Lett. 306, 137–148. https://doi.org/10.1016/j.epsl.2011.04.011.

North Greenland Ice Core Project members, 2004. High-resolution record of Northern Hemisphere climate extending into the last interglacial period. Nature 431, 147–151. https://doi.org/10.1038/nature02805.

Notz, D., Stroeve, J., 2018. The trajectory towards a seasonally ice-free Arctic Ocean. Curr. Clim. Change Rep. 4, 407–416. https://doi.org/10.1007/s40641-018-0113-2.

Ogawa, F., Spengler, T., 2019. Prevailing surface wind direction during air–sea heat exchange. J. Clim. 32, 5601–5617. https://doi.org/10.1175/JCLI-D-18-0752.1.

Olafsson, J., Olafsdottir, S.R., Takahashi, T., Danielsen, M., Arnarson, T.S., 2021. Enhancement of the North Atlantic CO2sink by arctic waters. Biogeosciences 18, 1689–1701. https://doi.org/10.5194/bg-18-1689-2021.

Onarheim, I.H., Eldevik, T., Smedsrud, L.H., Stroeve, J.C., 2018. Seasonal and regional manifestation of Arctic sea ice loss. J. Clim. 31, 4917–4932. https://doi.org/10.1175/JCLI-D-17-0427.1.

Parish, T.R., Cassano, J.J., 2003. Diagnosis of the katabatic wind influence on the wintertime antarctic surface wind field from numerical simulations. Mon. Weather Rev. 131, 1128–1139. https://doi.org/10.1175/1520-0493(2003)131<1128:DOTKWI>2.0.CO;2.

Parkinson, C.L., DiGirolamo, N.E., 2021. Sea ice extents continue to set new records: Arctic, Antarctic, and global results. Remote Sens. Environ. 267, 112753 https://doi.org/10.1016/j.rse.2021.112753.

Parmentier, F.J.W., Christensen, T.R., Sørensen, L.L., Rysgaard, S., Mcguire, A.D., Miller, P.A., Walker, D.A., 2013. The impact of lower sea-ice extent on Arctic greenhouse-gas exchange. Nat. Clim. Change 3, 195–202. https://doi.org/10.1038/nclimate1784.

Rasmussen, S.O., Bigler, M., Blockley, S.P., Blunier, T., Buchardt, S.L., Clausen, H.B., Cvijanovic, I., Dahl-Jensen, D., Johnsen, S.J., Fischer, H., Gkinis, V., Guillevic, M., Hoek, W.Z., Lowe, J.J., Pedro, J.B., Popp, T., Seierstad, I.K., Steffensen, J.P., Svensson, A.M., Vallelonga, P., Vinther, B.M., Walker, M.J.C., Wheatley, J.J., Winstrup, M., 2014. A stratigraphic framework for abrupt climatic changes during the Last Glacial period based on three synchronized Greenland ice-core records: refining and extending the INTIMATE event stratigraphy. Quat. Sci. Rev. 106, 14–28. https://doi.org/10.1016/j.quascirev.2014.09.007.

Rasmussen, T.L., Thomsen, E., 2004. The role of the North Atlantic Drift in the millennial timescale glacial climate fluctuations. Palaeogeogr. Palaeoclimatol. Palaeoecol. 210, 101–116. https://doi.org/10.1016/j.palaeo.2004.04.005.

Rheinlænder, J.W., Smedsrud, L.H., Nisanciouglu, K.H., 2021. Internal Ocean dynamics control the long-term evolution of weddell sea polynya activity. Frontiers in Climate 3. https://doi.org/10.3389/fclim.2021.718016.

Roche, D.M., Wiersma, A.P., Renssen, H., 2010. A systematic study of the impact of freshwater pulses with respect to different geographical locations. Clim. Dynam. 34, 997–1013. https://doi.org/10.1007/s00382-009-0578-8.

Sadatzki, H., Dokken, T.M., Berben, S.M.P., Muschitiello, F., Stein, R., Fahl, K., Menviel, L., Timmermann, A., Jansen, E., 2019. Sea ice variability in the southern Norwegian Sea during glacial Dansgaard-Oeschger climate cycles. Sci. Adv. 5 https://doi.org/10.1126/sciadv.aau6174.

Sadatzki, H., Maffezzoli, N., Dokken, T.M., Simon, M.H., Berben, S.M.P., Fahl, K., Kjær, H.A., Spolaor, A., Stein, R., Vallelonga, P., Vinther, B.M., Jansen, E., 2020. Rapid reductions and millennial-scale variability in Nordic Seas sea ice cover during abrupt glacial climate changes. Proc. Natl. Acad. Sci. USA 117, 29478–29486. https://doi.org/10.1073/pnas.2005849117.

Schneider, W., Budéus, G., 1997. Summary of the Northeast Water polynya formation and development (Greenland sea). J. Mar. Syst. 10, 107–122. https://doi.org/10.1016/S0924-7963(96)00075-9.

Scoto, F., Sadatzki, H., Maffezzoli, N., Barbante, C., Gagliardi, A., Varin, C., Vallelonga, P., Gkinis, V., Dahl-Jensen, D., Kjær, H.A., Burgay, F., Saiz-Lopez, A., Stein, R., Spolaor, A., 2022. Sea ice fluctuations in the Baffin Bay and the Labrador Sea during glacial abrupt climate changes. In: Proceedings of the National Academy of Sciences, vol. 119. https://doi.org/10.1073/pnas.2203468119.

Seierstad, I.K., Abbott, P.M., Bigler, M., Blunier, T., Bourne, A.J., Brook, E., Buchardt, S. L., Buizert, C., Clausen, H.B., Cook, E., Dahl-Jensen, D., Davies, S.M., Guillevic, M., Johnsen, S.J., Pedersen, D.S., Popp, T.J., Rasmussen, S.O., Severinghaus, J.P., Svensson, A., Vinther, B.M., 2014. Consistently dated records from the Greenland GRIP, GISP2 and NGRIP ice cores for the past 104 ka reveal regional millennial-scale δ18O gradients with possible Heinrich event imprint. Quat. Sci. Rev. 106, 29–46. https://doi.org/10.1016/j.quascirev.2014.10.032.

Sessford, E.G., Jensen, M.F., Tisserand, A.A., Muschitiello, F., Dokken, T., Nisancioglu, K. H., Jansen, E., 2019. Consistent fluctuations in intermediate water temperature off the coast of Greenland and Norway during Dansgaard-Oeschger events. Quat. Sci. Rev. 223 https://doi.org/10.1016/j.quascirev.2019.105887.

Sherriff-Tadano, S., Abe-Ouchi, A., Yoshimori, M., Oka, A., Chan, W.-L., 2018. Influence of glacial ice sheets on the Atlantic meridional overturning circulation through surface wind change. Clim. Dynam. 50, 2881–2903. https://doi.org/10.1007/s00382-017-3780-0.

Simon, M.H., Rutledal, S., Menviel, L., Zolles, T., Haflidason, H., Born, A., Berben, S.M.P., Dokken, T.M., 2023. Atlantic inflow and low sea-ice cover in the nordic seas promoted fennoscandian ice sheet growth during the last glacial Maximum. Commun Earth Environ 4. https://doi.org/10.1038/s43247-023-01032-9.

Smedsrud, L.H., Halvorsen, M.H., Stroeve, J.C., Zhang, R., Kloster, K., 2017. Fram Strait sea ice export variability and September Arctic sea ice extent over the last 80 years. Cryosphere 11, 65–79. https://doi.org/10.5194/tc-11-65-2017.

Smedsrud, L.H., Muilwijk, M., Brakstad, A., Madonna, E., Lauvset, S.K., Spensberger, C., Born, A., Eldevik, T., Drange, H., Jeansson, E., Li, C., Olsen, A., Skagseth, Ø., Slater, D.A., Straneo, F., Våge, K., Årthun, M., 2022. Nordic seas heat loss, atlantic inflow, and arctic Sea Ice cover over the last century. Rev. Geophys. https://doi.org/10.1029/2020RG000725.

Smik, L., Cabedo-Sanz, P., Belt, S.T., 2016. Semi-quantitative estimates of paleo Arctic sea ice concentration based on source-specific highly branched isoprenoid alkenes: a further development of the PIP25 index. Org. Geochem. 92, 63–69. https://doi.org/10.1016/j.orggeochem.2015.12.007.

Stap, L.B., van de Wal, R.S.W., de Boer, B., Bintanja, R., Lourens, L.J., 2014. Interaction of ice sheets and climate during the past 800 000 years. Clim. Past 10, 2135–2152. https://doi.org/10.5194/cp-10-2135-2014.

Stein, R., Fahl, K., Gierz, P., Niessen, F., Lohmann, G., 2017. Arctic Ocean sea ice cover during the penultimate glacial and the last interglacial. Nat. Commun. 8 https://doi.org/10.1038/s41467-017-00552-1.

Stoynova, V., Shanahan, T.M., Hughen, K.A., de Vernal, A., 2013. Insights into Circum-Arctic sea ice variability from molecular geochemistry. Quat. Sci. Rev. 79, 63–73. https://doi.org/10.1016/j.quascirev.2012.10.006.

Su, L., Ren, J., Sicre, M.A., Bai, Y., Jalali, B., Li, Z., Jin, H., Astakhov, A.S., Shi, X., Chen, J., 2022. HBIs and sterols in surface sediments across the East siberian sea: implications for palaeo sea-ice reconstructions. G-cubed 23.

Voelker, A.H.L., Grootes, P.M., Nadeau, M.-J., Sarnthein, M., 2000. Radiocarbon levels in the Iceland sea from 25–53 kyr and their link to the Earth's magnetic field intensity. Radiocarbon 42, 437–452. https://doi.org/10.1017/S0033822200030368.

Voelker, A.H.L., Haflidason, H., 2015. Refining the Icelandic tephrachronology of the last glacial period - the deep-sea core PS2644 record from the southern Greenland Sea. Global Planet. Change 131, 35–62. https://doi.org/10.1016/j.gloplacha.2015.05.001.

Volkman, J.K., 2006. Lipid markers for marine organic matter. Handb. Environ. Chem. 2 https://doi.org/10.1007/698_2_002. Reactions and Processes.

Volkman, J.K., 1986. A review of sterol markers for marine and terrigenous organic matter. Org. Geochem. 9, 83–99. https://doi.org/10.1016/0146-6380(86)90089-6.

Wadham, J.L., Hawkings, J.R., Tarasov, L., Gregoire, L.J., Spencer, R.G.M., Gutjahr, M., Ridgwell, A., Kohfeld, K.E., 2019. Ice sheets matter for the global carbon cycle. Nat. Commun. 10, 3567. https://doi.org/10.1038/s41467-019-11394-4.

Wary, M., Eynaud, F., Sabine, M., Zaragosi, S., Rossignol, L., Malaizé, B., Palis, E., Zumaque, J., Caulle, C., Penaud, A., Michel, E., Charlier, K., 2015. Stratification of surface waters during the last glacial millennial climatic events: a key factor in subsurface and deep-water mass dynamics. Clim. Past 11, 1507–1525. https://doi.org/10.5194/cp-11-1507-2015.

Wiberg, D.H., Haflidason, H., Laberg, J.S., 2022. An updated Weichselian chronostratigraphic framework of the Kongsfjorden Trough Mouth Fan and its implications for the glacial history of Svalbard. Boreas 51, 667–683. https://doi.org/10.1111/bor.12581.

Xiao, X., Fahl, K., Müller, J., Stein, R., 2015. Sea-ice distribution in the modern Arctic Ocean: biomarker records from trans-Arctic Ocean surface sediments. Geochim Cosmochim Acta 155, 16–29. https://doi.org/10.1016/J.GCA.2015.01.029.

Xiao, X., Fahl, K., Stein, R., 2013. Biomarker distributions in surface sediments from the Kara and Laptev seas (Arctic Ocean): indicators for organic-carbon sources and sea-ice coverage. Quat. Sci. Rev. 79, 40–52. https://doi.org/10.1016/j.quascirev.2012.11.028.

Zammett, R.J., Fowler, A.C., 2007. Katabatic winds on ice sheets: a refinement of the Prandtl model. J. Atmos. Sci. 64, 2707–2716. https://doi.org/10.1175/JAS3960.1.

Zeng, N., 2003. Glacial-interglacial atmospheric CO2 change —the glacial burial hypothesis. Adv. Atmos. Sci. 20, 677–693. https://doi.org/10.1007/BF02915395.

Zumaque, J., Eynaud, F., Zaragosi, S., Marret, F., Matsuzaki, K.M., Kissel, C., Roche, D. M., Malaizé, B., Michel, E., Billy, I., Richter, T., Palis, E., 2012. An ocean–ice coupled response during the last glacial: a view from a marine isotopic stage 3 record south of the Faeroe Shetland Gateway. Clim. Past 8, 1997–2017. https://doi.org/10.5194/cp-8-1997-2012.